Atmos. Chem. Phys. Discuss., 14, 22117–22153, 2014
www.atmos-chem-phys-discuss.net/14/22117/2014/
doi:10.5194/acpd-14-22117-2014

Atmospheric Chemistry and Physics Discussions

Quantifying contributions to the recent temperature variability in the tropical tropopause layer

W. Wang[1,2], **K. Matthes**[2], **and T. Schmidt**[3]

[1]Freie Universität Berlin, Institut für Meteorologie, Berlin, Germany
[2]GEOMAR Helmholtz-Zentrum für Ozeanforschung Kiel, Kiel, Germany
[3]Helmholtz Zentrum Potsdam, Deutsches GeoForschungsZentrum (GFZ), Potsdam, Germany

Received: 1 August 2014 – Accepted: 10 August 2014 – Published: 28 August 2014

Correspondence to: W. Wang (wuke.wang@fu-berlin.de)

Published by Copernicus Publications on behalf of the European Geosciences Union.

Abstract

The recently observed variability in the tropical tropopause layer, which features an unexpected warming of 1.1 K over the past decade (2001–2011), is investigated with a number of sensitivity experiments from simulations with NCAR's CESM-WACCM chemistry climate model. The experiments have been designed to specifically quantify the contributions from natural as well as anthropogenic factors, such as solar variability (Solar), sea surface temperatures (SSTs), the Quasi-Biennial Oscillation (QBO), stratospheric aerosols (Aerosol), greenhouse gases (GHGs), as well as the dependence on the vertical resolution in the model. The results show that, in the TTL: a cooling in tropical SSTs leads to a weakening of tropical upwelling around the tropical tropopause and hence relative downwelling and adiabatic warming of 0.3 K decade^{-1}; an increased QBO amplitude results in a 0.3 K decade^{-1} warming; increasing aerosols in the lower stratosphere lead to a 0.4 K decade^{-1} warming; a prolonged solar minimum and increased GHGs contribute about 0.2 and 0.1 K decade^{-1} to a cooling, respectively. Two simulations with different vertical resolution show that the vertical resolution can strongly influence the response of the TTL temperature to changes such as SSTs. With higher vertical resolution, an extra 0.6 K decade^{-1} warming can be simulated through the last decade, compared with results from the "standard" low vertical resolution simulation. Considering all the factors mentioned above, we compute a net 1.3 K decade^{-1} warming, which is in very good agreement with the observed 1.1 K decade^{-1} warming over the past decade in the TTL. The model results indicate that the recent warming in the TTL is mainly due to internal variability, i.e. the QBO and tropical SSTs.

1 Introduction

The tropical tropopause layer (TTL) is the transition layer from the upper troposphere to the lower stratosphere in the tropics, within which air has distinct properties of both the troposphere and the stratosphere. The vertical range of TTL depends on how it is

ACPD
14, 22117–22153, 2014

defined, i.e., it can be a shallower layer between 14–18.5 km (Fueglistaler et al., 2009) or a deeper layer of about 12–19 km (Gettelman and Forster, 2002; SPARC-CCMVal, 2010, chapter 7). As a key region for the stratosphere-troposphere coupling, TTL acts like a "gate" for air masses entering the stratosphere from the tropical troposphere. The coupling between dynamics, radiation and chemistry is especially strong in the TTL since it is the source region for trace gases entering into the stratosphere. The temperature in the TTL is determined by the combined influences of latent heat release, thermally as well as mechanically driven vertical motion, and radiative cooling (Gettelman and Forster, 2002; Fueglistaler et al., 2009; Grise and Thompson, 2013). The thermal structure, static stability and zonal winds in the TTL affect the two-way interaction between troposphere and stratosphere (Flury et al., 2013; Simpson et al., 2009) as well as surface climate, since the relative minimum temperature (usually known as the cold point tropopause, CPT) subsequently influences the radiation and water vapor budget (Andrews, 2010). The TTL reacts particularly sensitively to anthropogenically induced radiative, chemical and dynamical forcings of the climate system, and hence is a useful indicator of climate change (Fueglistaler et al., 2009).

Over the past decade, a remarkable warming has been captured by Global Positioning System Radio Occultation (GPS-RO) data in the TTL region (Schmidt et al., 2010; Wang et al., 2013, see also an extension in Fig. 2). This might indicate for a climate change signal, with possible important impacts on stratospheric climate, i.e., the tropical tropopause temperature dominates the water vapor entering the stratosphere (Dessler et al., 2013; Solomon et al., 2010; Gettelman et al., 2009; Randel and Jensen, 2013). Based on model simulations, Wang et al. (2013) suggested that the warming around the tropical tropopause could be a result of a weaker tropical upwelling, which implies a weakening of the Brewer–Dobson circulation (BDC). However, the strengthening or weakening of the BDC is still under debate (Butchart, 2014, and references therein). Results from observations indicate that the BDC may have slightly decelerated (Engel et al., 2009; Stiller et al., 2012), while estimates from a number of CCMs show in contrast a strengthening of the BDC (Butchart et al., 2010; Li et al., 2008). The

ACPD
14, 22117–22153, 2014

reason of the discrepancy between observed and modeled BDC changes, as well as the mechanism for changes in the BDC in response to climate change, is still under discussion (Oberländer et al., 2013; Shepherd and McLandress, 2011). The trends in the BDC may be different in the different branches of the BDC (Lin and Fu, 2013; Oberländer et al., 2013). Bunzel and Schmidt (2013) show that the model configuration, i.e. the vertical resolution and the vertical extent of the model, can also impact trends in the BDC.

There are a number of other natural and anthropogenic factors besides the BDC which influence the radiative, chemical and dynamical processes in the TTL. One prominent candidate for natural variability is the sun, which provides the energy source for the climate system. The 11 year solar cycle is the most prominent natural variation on the decadal time scale (Gray et al., 2010). Solar variability influences the temperature through direct radiative effects and indirectly through radiative effects on ozone as well as indirect dynamical effects. The maximum response in temperature occurs in the equatorial upper stratosphere during solar maximum conditions, and a distinct secondary temperature maximum can be found in the equatorial lower stratosphere around 100 hPa (SPARC-CCMVal, 2010; Gray et al., 2010). SSTs also influence the TTL by influencing the dynamical conditions and subsequently the propagation of planetary waves and circulation. Increasing tropical SSTs can enhance the BDC, which in turn cools the tropical lower stratosphere through enhanced upwelling (Grise and Thompson, 2012, 2013; Oberländer et al., 2013). The QBO is the dominant mode of variability throughout the equatorial stratosphere, and has important impacts on the temperature structure as well as the distribution of chemical constituents like water vapor, methane and ozone (Baldwin et al., 2001). Stratospheric aerosols warm the lower stratosphere by reflecting and scattering incident solar radiation back to space or by absorbing outgoing long-wave radiation, with a maximum aerosol heating around 20 km (Solomon et al., 2010; SPARC-CCMVal, 2010, chapter 8).

While GHGs warm the troposphere, they cool the stratosphere at the same time by releasing more radiation into space. Warming of the troposphere and cooling of the

ACPD
14, 22117–22153, 2014

stratosphere affect the temperature in the TTL directly, and also indirectly, by changing chemical trace gas distributions and wave activities (SPARC-CCMVal, 2010).

A sufficiently high vertical resolution is important in order for models to correctly represent dynamical process, such as wave propagation into the stratosphere and wave-mean flow interactions. It is a prominent factor for a climate model to generate a self-consistent QBO (Baldwin et al., 2001; Bunzel and Schmidt, 2013). Meanwhile, vertical resolution is essential to a proper representation of the thermal structure in the model, e.g. models with coarse vertical resolution can not simulate the tropopause inversion layer (TIL, a narrow band of temperature inversion above the tropopause associated with a region of enhanced static stability) well (Wang et al., 2013; SPARC-CCMVal, 2010, chapter 7). Coarse vertical resolution is also still a problem for analysing the effects of El-Niño Southern Oscillation (ENSO) and the QBO onto the tropical tropopause (Zhou et al., 2001; SPARC-CCMVal, 2010, chapter 7).

Here we use a series of simulations with NCAR's Community Earth System Model (CESM) model (Marsh et al., 2013), to quantify the contributions of the above discussed factors-Solar, SSTs, QBO, Aerosol and GHGs-to the recently observed variability in the TTL.

The details of the observed data, the model and numerical experiments, as well as a description of our methods are given in Sect. 2. The observed temperature variability in the TTL and the contributions of various factors to the recent TTL variability are addressed in Sect. 3. Section 4 focuses on the importance of the vertical resolution in one climate model. A summary and discussion are presented in Sect. 5.

2 Model simulations and method description

2.1 Fully-coupled CESM-WACCM simulations

The model used here is NCAR's Community Earth System Model (CESM) model, version 1.0. CESM is a fully coupled model system, including an interactive ocean (POP2),

ACPD
14, 22117–22153, 2014

land (CLM4), sea ice (CICE) and atmosphere (CAM/WACCM) component (Marsh et al., 2013). As atmospheric component we use the Whole Atmosphere Community Climate Model (WACCM), version 4. WACCM4 is a chemistry climate model (CCM), with detailed middle atmospheric chemistry and a finite volume dynamical core, extending from the surface to about 140 km (Marsh et al., 2013). The standard version has 66 (W_L66) vertical levels, which means about 1 km vertical resolution in the TTL and the lower stratosphere. All the simulations use a horizontal resolution of $1.9^{\circ} \times 2.5^{\circ}$ (latitude × longitude) for the atmosphere and approximately 1 degree for the ocean.

Table 1 gives an overview of all coupled CESM simulations. A control run was performed from 1955 to 2100 (Natural run hereafter), with all natural forcings including spectrally resolved solar variability (Lean et al., 2005), a fully coupled ocean, volcanic aerosols according to CCMVal2 recommendations (Morgenstern et al., 2010) and nudged QBO (see details in Matthes et al., 2010; Hansen et al., 2013). The solar variability and volcanic aerosols used here follow the SPARC CCMVal REF-B2 scenario (see details in SPARC-CCMVal, 2010). Anthropogenic forcings like GHGs and ozone depleting substances (ODSs) are set to constant 1960s conditions. Using the Natural run as a reference, a series of four sensitivity experiments were performed by systematically switching on or off several factors. The SolarMean run uses constant solar cycle values averaged over past observed solar cycles; the FixedSST run uses monthly varying climatological SSTs calculated from the Natural run, and therefore neglects variability from varying SSTs such as ENSO; in the NOQBO run the QBO nudging has been switched off which means weak zonal mean easterly winds develop in the tropical stratosphere. An additional simulation RCP85, uses the same forcings as the Natural run, but in addition includes anthropogenic GHGs and ODSs forcings. These forcings are based on observations from 1955 to 2005, after which they follow the Representative Concentration Pathways (RCPs) RCP8.5 scenario (Meinshausen et al., 2011).

ACPD
14, 22117–22153, 2014

2.2 WACCM atmospheric stand-alone simulations

Instead of using the fully coupled CESM-WACCM version, WACCM can be integrated in an atmospheric stand-alone configuration, with prescribed SSTs and sea ice. Beside the standard version with 66 vertical levels (W_L66), we have also performed simulations with a finer vertical resolution, with 103 vertical levels and about 300 m vertical resolution in the TTL and lower stratosphere (W_L103) (Gettelman and Birner, 2007; Wang et al., 2013).

With the stand-alone atmospheric version an ensemble of three experiments was performed over the recent decade 2001–2010 with both WACCM versions (W_L66, W_L103) (see Table 2). Observed SSTs and spectrally resolved solar fluxes were used to produce the most realistic simulations of atmospheric variability over the past decade (2001–2010). GHGs and ODSs are based on observations for the first 5 years (2001–2005) and then follow the IPCC RCP4.5 scenario for the next 5 years (2005–2010), since no observed data were available when the simulations were started. Atmospheric aerosols were relatively constant between 2001 and 2010 since no strong volcanic eruptions occurred, and are the same in the CESM-WACCM runs described above. All the forcings considered in this study are available from the CESM model input data repository (https://svn-ccsm-inputdata.cgd.ucar.edu/trunk/inputdata/). The results presented in the following are ensemble averages for each of the two WACCM vertical resolution versions. An additional run (W_Aerosol) was performed using the W_L103 version with observed, more realistic stratospheric aerosol forcings from the Chemistry-Climate Model Initiative (CCMI, http://www.met.reading.ac.uk/ccmi/) project.

2.3 Linear trend calculation

A standard least square regression is used to calculate the linear trend. For example, using time (t) as a single predictor, the predicted temperature (T) can be expressed as:

$$T_{\text{est}} = a + bt, \quad (1)$$

ACPD
14, 22117–22153, 2014

where the subscript "est" indicates that this is an estimate of T, and "b" represents the linear trend. The residuals are defined by the differences between the actual and the estimated temperature

$$e = T - T_{\text{est}}. \quad (2)$$

The "best-fit" is defined by the line that minimizes the sum of the squares of the residuals. The seasonal cycle was removed from the temperature time series before doing the regression.

The standard error (SE) is used to estimate the uncertainty of the estimated trend, which is defined by:

$$(\text{SE})^2 = \left[\sum e^2\right] / (n-2) / \left[\sum \left((t - \bar{t})^2\right)\right], \quad (3)$$

where n is the sample size, and $\bar{t}$ is the mean value. The smaller this standard error is, the more certain is the trend.

If the trend is larger than two times the standard error, the linear regression is statically significant at the 95 % confidence level. A brief description of the least square regression, the uncertainty of the trend, as well as the significance testing can be found in Wigley (2006).

2.4 Composite method

To estimate the contribution of the different factors to the observed temperature variability in the TTL, the composite for each factor is computed following three steps: (1) calculation of the linear trend for the respective factor over the past decade (2001–2011) from the observed, deseasonalized time series, (2) selection of time periods in the reference run, which are similar to the observed trends for the respective factor (the method of selection and the number of similar time periods depends on the factor, see below), and (3) calculation of the linear temperature trends for each selected time period, followed by averaging of all trend periods together to obtain a composite trend.

ACPD
14, 22117–22153, 2014

The composite trend is calculated for both each reference run and the run to which it is compared. Both runs have the same configuration and forcings, except for the long-term variability of the respective factor. The contribution of this factor is then quantified by the difference between the reference run and the run without this factor.

The difference of the trend between two runs is simply the difference time series, i.e. subtracting the time series of the reference run from the run to which it is compared. The uncertainty and the significance of the trend difference between two runs are then estimated by the standard error of the regression in the difference time series and the comparison between the trend and the standard error.

The uncertainty of the composite trend is estimated by the mean of the standard errors in different selected time periods. The significance of the composite trend is then tested by a comparison between the composite trend and the mean of the standard error.

Special attention is given to the region 20° S–20° N latitude and 16–18.5 km height, which is almost exactly the TTL region (Fueglistaler et al., 2009). Hereafter, we use the term "temperature trend" in the TTL to indicate the average trend over this area. Afterwards the exact contribution of every factor can be quantified. The uncertainty of each contribution is the mean value of the standard error in that region.

Figure 1 shows the time series of both natural and anthropogenic forcings over past and future decades in the observations (black) and in the Natural model experiment (blue). Periods with a similar trend as the recent decade (2001–2011) are shown with straight lines.

Observations of the solar variability show that the total solar irradiance (TSI) exhibits a clear 11 year solar cycle (SC) variation of about 1 W m^{-2} between sunspot minimum (S_{min}) and sunspot maximum (S_{max}) in the past (Gray et al., 2010), with a delayed and smaller amplitude return to maximum conditions in the recent decade (Fig. 1a). The future projection is a repetition of the last four observed solar cycles. Similar periods of decreasing TSI can be found in the periods 1958–1968, 2001–2011, 2045–2055, and 2089–2099. A composite trend is then constructed by averaging over all four selected

ACPD
14, 22117–22153, 2014

periods in the Natural as well as the SolarMean experiments. By comparing the trends in these two runs with and without solar cycle variations, the effect of solar variability on the temperature trend in the TTL can be estimated.

Figure 1b shows the variability of tropical (20° S–20° N) SSTs for the recent past from observations (Hadley Center Updates and supplementary information available from http://www.metoffice.gov.uk/hadobs/hadisst, black lines) and up to 2100 from the Natural coupled CESM-WACCM model experiment (blue lines). Both the observed and simulated tropical SSTs show a statistically significant (over 95 %) decrease from 2001 to 2011. A similar decrease in tropical SSTs can be found during the periods 1956–1968, 1980–1991, 2001–2014, 2028–2043 and 2047–2057. Periods longer than 10 years each has been selected from the filtered tropical SST time series. Filtering has been performed twice with a Butterworth low-pass filter (longer than 30 years). Afterwards a composite trend was constructed by averaging over the five selected time periods. Note that there is also a strong drop in SSTs around 1992 in the model, which does not occur in the observations. This might be caused by an overestimated response to the Pinatubo eruption in CESM-WACCM (Marsh et al., 2013; Meehl et al., 2012). By comparing the Natural run, where SSTs are calculated explicitly, and the FixedSST run where SSTs are climatologically prescribed, the effect of interactively calculated SSTs can be determined.

Instead of a decrease in tropical SSTs, the QBO amplitude shows an increase during the selected two periods (Fig. 1c). The observed QBO amplitude has been calculated from the absolute values of deseasonalized monthly mean anomalies of the zonal mean zonal wind at 70 hPa (from the FU Berlin: http://www.geo.fu-berlin.de/en/met/ag/strat/produkte/qbo/index.html); in our model simulations it is computed where the QBO has been nudged. The time periods of increasing QBO amplitude are selected by the same as the procedure as for the tropical SSTs. By comparing the Natural and the NOQBO experiments, the effect of a (nudged) QBO on the temperature trends in the TTL can be estimated.

ACPD
14, 22117–22153, 2014

As shown in Fig. 1d, GHGs show a steady increase after 2001. The increasing rate of global CO_2 release from 2001 to 2011 is close to the RCP8.5 scenario, which we used in our RCP85 run. By comparing the experiments with (RCP8.5) and without (Natural) GHG increases, the GHG effect on the observed temperature trend can be estimated. Similar to the GHGs, observed stratospheric aerosols (aerosol optical depth (AOD)) have been steadily increasing since 2001 (Solomon et al., 2010) in the lower stratosphere (18–32 km) (Fig. 1e). This increase in stratospheric aerosol loading is attributed to a number of small volcanic eruptions and anthropogenically released aerosols transported into the stratosphere during the Asia Monsoon (Bourassa et al., 2012; Neely et al., 2013). An aerosol data set has been constructed for the CCMI project (ftp://iacftp.ethz.ch/pub_read/luo/ccmi/) and is similar to the data described by Solomon et al. (2010). The comparison of the two experiments with different AOD data sets will shed light on the stratospheric aerosol contribution to the observed temperature trend.

All natural and anthropogenic forcings will be discussed with respect to their contribution to the temperature variability in TTL in the following section.

3 Quantification of observed temperature variability

3.1 Observed temperature variability in the TTL

Figure 2 shows the latitude-height section of the linear temperature trend for the period 2001–2011 estimated from GPS-RO observations (see details of the GPS-RO data in Wang et al., 2013). A remarkable and statistically significant warming occurs around the TTL between about 20° south to north and from 15 to 20 km height. The warming in the TTL is $1.1 \pm 0.2\,\mathrm{K\,decade^{-1}}$ on average, with a maximum of about $1.8\,\mathrm{K\,decade^{-1}}$ directly at the tropical tropopause around 17 to 18 km. The uncertainty is given by the standard error of the trend as described in Sect. 2.4. This figure is an extension of earlier work by Schmidt et al. (2010) and Wang et al. (2013) and shows an unexpected

ACPD
14, 22117–22153, 2014

warming, despite the steady increase in GHGs which imply a cooling of this region. Therefore it is interesting to study whether this warming is simply a phenomenon of the past decade and the result of internal atmospheric variability, or whether it will persist for longer and therefore modify trace gas transport from the troposphere into the stratosphere.

3.2 Contribution of solar variability

Figure 3a and b shows the composite temperature trends for periods with decreasing solar irradiance (1958–1968, 2001–2011, 2045–2055, and 2089–2099) for the Natural and SolarMean runs, respectively. The Natural run shows an insignificant temperature increase from S_{max} to S_{min} of about 0.2 K decade^{-1} around the tropical tropopause, and a decrease at the tropical lower stratosphere, while the SolarMean run shows a partially statistically significant temperature increase between 0.2 and 0.6 K decade^{-1} in the tropics and subtropics. Figure 3c shows the differences in temperature trends between the Natural run and the SolarMean experiments. Solar variability thus contributed to a cooling of 0.2 ± 0.2 K decade^{-1} in the TTL between 2001 and 2011. The relatively large uncertainty in the combined temperature trend indicates that there are large uncertainties in the estimated contribution due to solar variability.

3.3 Contribution of tropical SSTs

Figure 4 shows the composite temperature trends for the periods with decreasing tropical SSTs (1956–1968, 1980–1991, 2001–2014, 2028–2043 and 2047–2057) for both the Natural and the FixedSST runs (Fig. 4a and b), as well as their differences (Fig. 4c). While the Natural experiment shows a partially statistically significant temperature increase of 0.4 K decade^{-1} on average maximally 0.8 K decade^{-1} in the TTL, the FixedSST experiment shows only all insignificant (0–0.2 K decade^{-1}) warming during the recent decade. A decrease in tropical SSTs contributes therefore to a statistically significant warming of 0.3 ± 0.2 K decade^{-1} on average (0.6 K decade^{-1} in maximum)

ACPD
14, 22117–22153, 2014

in the TTL (Fig. 4c). The uncertainty in the combined temperature trend reveals relative small uncertainties from the contribution of tropical SSTs.

3.4 Contribution of the QBO

Figure 5a and b shows the composite temperature trends, for periods with increasing QBO amplitudes (2003–2017 and 2054–2068) for the Natural and the NOQBO experiment, respectively. While the Natural experiment shows a warming of 0.2 K decade^{-1} on average maximally 0.8 K decade^{-1} in the TTL, the NOQBO run shows a slight cooling for the same period. The differences in Fig. 5c indicate that the increased QBO amplitude contributes to a warming of 0.3 ± 0.2 K decade^{-1} on average (0.8 K decade^{-1} in maximum) in the TTL. The uncertainty in the composite temperature trend indicates a relatively small uncertainty in the QBO contribution to TTL temperature. Another effect of the QBO is the statistically significant cooling trend seen in the tropical middle stratosphere above 22 km in the Natural run. This QBO effect may help to explain the observed tropical cooling (see Fig. 2). Please note, however, that, the CESM1.0, which was used for these simulations, can not generate a self-consistent QBO and hence uses wind nudging, which might cause problems when estimating QBO effects on temperature variability in the tropical lower stratosphere (Marsh et al., 2013; Morgenstern et al., 2010).

3.5 Contribution of GHGs

The temperature trends from both the Natural and the RCP85 experiments between 2001 and 2011 are shown in Fig. 6a and b, respectively. As expected, increasing GHGs in the RCP8.5 experiment tends to cool the TTL, whereas the contribution from the run with fixed GHG conditions is slightly positive. Hence the effect of global warming is seen in Fig. 6c with a clear cooling trend in the TTL of about 0.1 ± 0.2 K decade^{-1}. The uncertainty of the GHGs contribution is relatively large. Figure 6c shows that the GHGs

ACPD
14, 22117–22153, 2014

do not affect the TTL temperatures much, but contribute instead to a cooling at upper levels in the lower stratosphere.

3.6 Contribution of stratospheric aerosols

The temperature trends from the simulations with relative constant AOD values (W_L103) and with more realistic CCMI aerosols (W_Aerosol) are shown in Fig. 7a and b, respectively. A clearly stronger and more statistically significant warming pattern can be seen around the tropical tropopause in the W_Aerosol run compared to the W_L103 run. The effect of increasing stratospheric aerosols is estimated to be 0.4 $\pm$ 0.2 K decade^{-1} warming in the TTL (Fig. 7c). The uncertainty of the contribution due to stratospheric aerosol is relatively small.

4 Effect of the vertical resolution

To estimate not only anthropogenic and natural contributions to the recent TTL temperature variability but also the effects of the vertical resolution in the model, Fig. 8a and b shows the temperature trends in the standard W_L66 run and the differences in temperature trends between the high-resolution (W_L103) and the standard (W_L66) runs, respectively. The W_L103 run (Fig. 7a) shows a statistically significant warming over the past decade around the TTL, which maximizes at 1 K decade^{-1}. The standard W_L66 run (Fig. 8a) does not capture the warming. The only difference between the two experiments is the vertical resolution, meaning that a higher vertical resolution captures the warming in the TTL better than the standard vertical resolution, reaching up to 0.6 $\pm$ 0.2 K decade^{-1} (Fig. 8b). The uncertainty of the effect of vertical resolution is relatively small. Wang et al. (2013) showed that the tropical upwelling in the lower stratosphere has weakened over the past decade in the W_L103 run, while there is no significant upwelling trend in the standard vertical resolution (W_L66) run. The decreasing tropical upwelling in the W_L103 run might be the reason for the extra

ACPD
14, 22117–22153, 2014

warming in the TTL compared to the W_L66 run, since dynamical changes would lead to adiabatic warming.

4.1 Changes in wave-mean flow interaction

To investigate dynamical differences between the two experiments with standard and higher vertical resolution in more detail, the Transformed Eulerian Mean (TEM) diagnostics (Andrews et al., 1987) were applied to investigate differences in the wave propagation and wave-mean flow interactions in the climatological mean as well as in the decadal trend. The Eliassen–Palm flux (EP flux) vector shows the direction of wave propagation, and its divergence is a measure of wave-mean flow interactions. Figure 9 features the climatology of annual means of the EP flux vector (errors), the divergence of the EP flux vector (shading), and the zonal mean zonal wind (contours) from the W_L103 run (Fig. 9a), as well as the differences for each variable between the W_L103 and the W_L66 runs (Fig. 9b). Also shown are the trends for each variable in Fig. 9a from the W_L103 run (Fig. 9c) and the differences in the trends between the W_L103 and the W_L66 runs (Fig. 9d).

Figure 9a shows extratropical wave propagation upward from the lower to the upper troposphere and lower stratosphere in mid-latitudes, and an equatorward propagation of waves in the vicinity of the tropospheric subtropical jet, where some of the waves dissipate (divergence regions) (Fig. 9a). At the same time, equatorial waves propagate from the tropical lower troposphere to the tropopause region. In the finer vertical resolution (W_L103) experiment, the upward EP flux from the mid-latitude troposphere is stronger than in the standard vertical resolution (W_L66) experiment in the middle to upper troposphere. The upward directed equatorial waves are also stronger because of the higher vertical resolution. Although upward propagation from both the mid-latitudes and tropics strengthens in the upper troposphere, waves are damped around the tropopause because the upper part of the subtropical jets is about 2.5 m s^{-1} weaker. Especially in the mid-latitude upper troposphere (12–16 km), there is a significant strengthening (weakening) of wave propagation from the extratropics to the tropics

ACPD
14, 22117–22153, 2014

(from the tropics to the extratropics). At the same time, there is a stronger downward wave propagation in the tropical lower stratosphere (16–20 km). In summary, a finer vertical resolution leads to a stronger tropical upwelling from the lower to the upper troposphere (in the W_L103 as compared to the W_L66 experiment) in the climatological annual mean, but a weaker tropical upwelling in the lower stratosphere (see also discussion below).

The annual mean trend in the above discussed quantities is depicted in Fig. 9c for the high vertical resolution experiment. During the past decade significantly more waves propagated from the mid-latitudes into the tropics in the W_L103 experiment. This strengthening of wave propagation from higher latitudes to the tropics is most visible in the tropical upper troposphere between 11–17 km, and above the tropopause in the lower stratosphere above 18 km. There is also a trend towards slightly enhanced downward propagation around the TTL coinciding with a significant divergence of the EP flux in this region. A weaker upwelling in the mid to high latitude upper troposphere to lower stratosphere occurs in both hemispheres. A stronger upward propagation occurs in the tropical upper troposphere until about 12 km. Compared with the simulation in standard vertical resolution (run W_L66), the W_L103 run shows a stronger weakening of the upward wave propagation from the mid-to-high latitude upper troposphere to the lower stratosphere (Fig. 9d). In the tropical troposphere below 12 km, the strengthening of the upward propagation is much weaker in the run W_L103 compared with the W_l66 experiment in the Southern Hemisphere, but is stronger in the Northern Hemisphere. How changes in the wave propagation affect the Brewer–Dobson circulation and hence temperature anomalies will be discussed in the following section.

4.2 Changes in the Brewer–Dobson circulation

Figure 10 shows the annual mean climatology of the Brewer–Dobson circulation (BDC) (arrows for the meridional and vertical wind components), and the temperature from the W_L103 run (Fig. 10a), as well as the differences between the W_L103 and the W_L66 runs (Fig. 10b). The BDC shows an upwelling in the tropics and a downwelling through

ACPD
14, 22117–22153, 2014

mid to high latitudes in the annual mean. With finer vertical resolution (W_L103) the model produces a stronger upwelling in the tropics (and a consistent cooling) up to the upper troposphere at around 16 km and in the tropical lower stratosphere. Around the tropical tropopause there is less upwelling and in particular more transport from the subtropics into the tropical TTL, leading to a stronger warming around 19 km in the W_L103 experiment. The stronger and statistically significant warming in the mid-latitude troposphere around 13 km on both hemispheres corresponds to stronger transport from the tropics to the mid latitudes. These changes in the BDC indicate a strengthening of its transit branch (Lin and Fu, 2013), and a weakening of the upper branch. This is consistent with previous work by Bunzel and Schmidt (2013), which indicates a weaker upward mass flux over 70 hPa in a model experiment with higher vertical resolution.

The annual mean trends in the W_L103 experiment indicate a further strengthening of the BDC transit branch over the past decade in this simulation (Fig. 10c) and a statistically significant weakening of the upper branch resulting in significant warming of 1 to 2 K decade^{-1} in the TTL. In addition, there is a statistically significant weakening of the downwelling over the Southern Hemisphere high latitudes, which results in a statistically significant cooling over the south polar region. In particular the trends in the TTL are stronger in the W_L103 compared to the W_L66 experiment (Fig. 10d). This is consistent with previous work by Bunzel and Schmidt (2013), which shows also stronger changes in BDC using a model with higher vertical resolution.

In summary, the finer vertical resolution can enhance the upward wave propagation from both tropics and extratropics. This enhanced wave propagation speeds up the transit branch of the BDC in the upper troposphere and slows down the lower stratospheric branch of the BDC. These changes in the BDC and corresponding wave-mean flow interactions (see above) finally result in the statistically significant warming in the TTL.

Bunzel and Schmidt (2013) attributed the differences in BDC to different vertical resolutions which tend to reduce the numerical diffusion through the tropopause and the

ACPD
14, 22117–22153, 2014

secondary meridional circulation. Our results show that the strong warming and subsequent enhanced static stability (not shown) above the tropopause may also influence wave dissipation and propagation around the tropopause. Due to Oberländer et al. (2013), the strengthening of BDC from the past to the future is mainly caused by an increase of tropical SSTs. Our results show a weakening of the upper branch of the BDC in the lower stratosphere following a decline in tropical SSTs, and thereby support earlier work. At the same time, a stronger warming in the TTL, due to a stronger weakening of the BDC in simulations with higher vertical resolution indicates that, with finer vertical resolution, the model can also produce a better response of long-term variability in the TTL due to surface changes such as changes in tropical SSTs.

5 Summary

Based on a series of sensitivity simulations with NCAR's CESM-WACCM model, the contribution of different natural (solar, QBO, tropical SSTs) and anthropogenic (GHGs, ODS) factors to the observed warming of the TTL over the past decade from 2001 through 2011 has been studied. By comparing model experiments with and without the respective factors and combining a number of periods with similar trends in a composite, the contribution of each factor has been quantified in order to explain the causes of the observed recent decadal variability in GPS-RO data.

A decrease in tropical SSTs, an increase in stratospheric aerosol loading and an increase in the QBO amplitude contribute each about 0.3, 0.4 and 0.3 K decade^{-1} to this warming, respectively, resulting in a total 1.0 K decade^{-1} warming, while the delay and smaller amplitude of the current solar maximum and the steady increase in GHGs and ODS concentrations contribute each about 0.2 and 0.1 K decade^{-1} to a cooling, respectively, resulting in a total 0.3 K decade^{-1} cooling. The vertical resolution of the model strongly influences the TTL response to the surface mainly via dynamical changes, i.e. an enhancement of the (lower) transit branch of the BDC and a decrease of the upper branch in response to the decreasing tropical SSTs. This leads to a 0.6 K decade^{-1}

ACPD
14, 22117–22153, 2014

extra warming in the TTL in the finer vertical resolution experiment as compared to the standard vertical resolution. Summing all natural and anthropogenic factors, as well as the contribution from finer vertical resolution, we arrive at a total modeled warming of 1.3 K decade^{-1} around the TTL, which is in very good agreement with the observed 1.1 K decade^{-1} warming from GPS-RO data. Although this is a very good agreement, care must be taken, since in reality non-linear interactions between the different factors might occur which we did not take into consideration in our first order linear approach. This uncertainty from the non-linear interactions should relatively small, which can be supported by our W_Aerosol run. The W_Aerosol run, with almost all observed forcings considered in this study, can be seen as the most realistic simulation. The TTL warming in the W_Aerosol run is 1.0 K decade^{-1} on average and 1.6 K decade^{-1} in maximum (Fig. 7b), which is very close to both the observed and composite temperature trend.

According to our experiments, one of the primary factors contributing to the recent warming in the TTL is the natural variability in tropical SSTs. A change in the sign of tropical SST tendency, for example an SST increase from 1960 through 2000 (Randel et al., 2009) and a decrease since 2001, leads to an opposite change in sign for TTL temperature tendency, which means a cooling from about 1960 to 2000 and a warming after 2001. However, the mechanism for this change in sign in the SSTs tendency, as well as the response of the TTL awaits further investigation. Our simulations indicate that the vertical resolution in the upper troposphere and lower stratosphere seems to be a key factor in simulating the response of TTL variability to SST changes accurately.

A similar change in sign can be seen in the trends of the QBO amplitude, which shows a decrease from about 1960 to 2000 but an increase since 2001. The long-term trend in QBO amplitude has been attributed by Kawatani and Hamilton (2013) to the variability in tropical upwelling near the tropical tropopause. However, the influences of this changing QBO amplitude on the temperature variability in the TTL is still unclear. Here, we made a simple estimation of this influence using a comparison between two simulations. There are still relatively large uncertainties in our estimation because of the nudged QBO in our model instead of a self-consistent QBO. The similar

ACPD
14, 22117–22153, 2014

TTL temperature changes for long-term variability due to changes in tropical SSTs and QBO amplitude suggest that they are closely related to each other. A lagged correlation has been made for the time series of the QBO and the tropical SSTs from 1960 to 2000 (not shown). We find that a 0.6 correlation coefficient, with a lead time of about two years in tropical SSTs, which indicates that the SSTs may lead to the observed QBO long-term variability.

Another recent interesting signal of climate change can be found at the surface: the Earth's global average surface air temperature has stalled since around 2001 despite ongoing increases of atmospheric GHGs (Balmaseda et al., 2013; England et al., 2014; Fyfe and Gillett, 2014; Kosaka and Xie, 2013). The proposed causes for this strange behaviour include a decrease in solar variability, increasing water vapor concentrations or stratospheric aerosol loading, the strengthening of the Pacific trade winds and the enhanced heat transport from the surface to ocean depths over the past decade (England et al., 2014; Kosaka and Xie, 2013; Fyfe et al., 2013). A change in the sign of temperature tendency at around 2001, both at the surface and in the TTL, suggests that the surface and the TTL are closely related to each other. Understanding the mechanism for changes in the TTL can therefore help to understand the mechanisms for the global warming hiatus, but needs further detailed investigation.

The external forcings (solar, GHGs, ODS) contribute relatively little to the temperature variability in the TTL, except for the stratospheric aerosols. Internal variability, i.e. the QBO and tropical SSTs, seem to be mainly responsible for the recent TTL warming.

Acknowledgements. W. Wang is supported by a fellowship of the China Scholarship Council (CSC) at FU Berlin. This work was also performed within the Helmholtz-University Young Investigators Group NATHAN, funded by the Helmholtz-Association through the president's Initiative and Networking Fund, and the GEOMAR – Helmholtz-Zentrum für Ozeanforschung in Kiel. The model calculations have been performed at the Deutsche Klimarechenzentrum (DKRZ) in Hamburg, Germany. We thank C. Petrick, F. Hansen, R. Thiéblemont and S. Wahl for carrying out some of the simulations. We thank L. Neef for grammar checking.

ACPD
14, 22117–22153, 2014

The service charges for this open access publication have been covered by a Research Centre of the Helmholtz Association.

References

Andrews, D. G.: An Introduction to Atmospheric Physics, Cambridge University Press, New York, 2010. 22119

Andrews, D. G., Holton, J. R., and Leovy, C. B.: Middle Atmosphere Dynamics, vol. 40, Academic Press, San Diego, 1987. 22131

Baldwin, M. P., Gray, L. J., Dunkerton, T. J., Hamilton, K., Haynes, P. H., Randel, W. J., Holton, J. R., Alexander, M. J., Hirota, I., Horinouchi, T., Jones, D. B. A., Kinnersley, J. S., Marquardt, C., Sato, K., and Takahashi, M.: The quasi-biennial oscillation, Rev. Geophys., 39, 179–229, doi:10.1029/1999RG000073, 2001. 22120, 22121

Balmaseda, M. A., Trenberth, K. E., and Källén, E.: Distinctive climate signals in reanalysis of global ocean heat content, Geophys. Res. Lett., 40, 1754–1759, doi:10.1002/grl.50382, 2013. 22136

Bourassa, A. E., Robock, A., Randel, W. J., Deshler, T., Rieger, L. A., Lloyd, N. D., Llewellyn, E. T., and Degenstein, D. A.: Large volcanic aerosol load in the stratosphere linked to Asian monsoon transport, Science, 337, 78–81, doi:10.1126/science.1219371, 2012. 22127

Bunzel, F. and Schmidt, H.: The Brewer–Dobson circulation in a changing climate: impact of the model configuration, J. Atmos. Sci., 70, 1437–1455, doi:10.1175/JAS-D-12-0215.1, 2013. 22120, 22121, 22133

Butchart, N.: The Brewer–Dobson circulation, Rev. Geophys., 52, 157–184, doi:10.1002/2013RG000448, 2014. 22119

Butchart, N., Cionni, I., Eyring, V., Shepherd, T. G., Waugh, D. W., Akiyoshi, H., Austin, J., Bruhl, C., Chipperfield, M. P., Cordero, E., Dameris, M., Deckert, R., Dhomse, S., Frith, S. M., Garcia, R. R., Gettelman, A., Giorgetta, M. A., Kinnison, D. E., Li, F., Mancini, E., McLandress, C., Pawson, S., Pitari, G., Plummer, D. A., Rozanov, E., Sassi, F., Scinocca, J. F., Shibata, K., and Tian, W.: Chemistry-climate model simulations of twenty-first century stratospheric

ACPD
14, 22117–22153, 2014

climate and circulation changes, J. Climate, 23, 5349–5374, doi:10.1175/2010JCLI3404.1, 2010. 22119

Dessler, A. E., Schoeberl, M. R., Wang, T., Davis, S. M., and Rosenlof, K. H.: Stratospheric water vapor feedback., P. Natl. Acad. Sci. USA, 110, 18087–18091, doi:10.1073/pnas.1310344110, 2013. 22119

Engel, A., Mobius, T., Bonisch, H., Schmidt, U., Heinz, R., Levin, I., Atlas, E., Aoki, S., Nakazawa, T., Sugawara, S., Moore, F., Hurst, D., Elkins, J., Schauffler, S., Andrews, A., and Boering, K.: Age of stratospheric air unchanged within uncertainties over the past 30 years, Nat. Geosci., 2, 28–31, doi:10.1038/ngeo388, 2009. 22119

England, M. H., McGregor, S., Spence, P., Meehl, G. A., Timmermann, A., Cai, W., Gupta, A. S., McPhaden, M. J., Purich, A., and Santoso, A.: Recent intensification of wind-driven circulation in the Pacific and the ongoing warming hiatus, Nature Climate Change, 4, 222–227, doi:10.1038/nclimate2106, 2014. 22136

Flury, T., Wu, D. L., and Read, W. G.: Variability in the speed of the Brewer–Dobson circulation as observed by Aura/MLS, Atmos. Chem. Phys., 13, 4563–4575, doi:10.5194/acp-13-4563-2013, 2013. 22119

Fueglistaler, S., Dessler, A., Dunkerton, T., Folkins, I., Fu, Q., and Mote, P. W.: Tropical tropopause layer, Rev. Geophys., 47, 1004, doi:10.1029/2008RG000267, 2009. 22119, 22125

Fyfe, J. C. and Gillett, N. P.: Recent observed and simulated warming, Nature Clim. Change, 4, 150–151, doi:10.1038/nclimate2111, 2014. 22136

Fyfe, J. C., Gillett, N. P., and Zwiers, F. W.: Overestimated global warming over the past 20 years, Nature Climate Change, 3, 767–769, doi:10.1038/nclimate1972, 2013. 22136

Gettelman, A. and Birner, T.: Insights into tropical tropopause layer processes using global models, J. Geophys. Res., 112, D23104, doi:10.1029/2007JD008945, 2007. 22123

Gettelman, A. and Forster, P. D. F.: A climatology of the tropical tropopause layer, J. Meteor. Soc. Jpn., 80, 911–924, doi:10.2151/jmsj.80.911, 2002. 22119

Gettelman, A., Birner, T., Eyring, V., Akiyoshi, H., Bekki, S., Brühl, C., Dameris, M., Kinnison, D. E., Lefevre, F., Lott, F., Mancini, E., Pitari, G., Plummer, D. A., Rozanov, E., Shibata, K., Stenke, A., Struthers, H., and Tian, W.: The Tropical Tropopause Layer 1960–2100, Atmos. Chem. Phys., 9, 1621–1637, doi:10.5194/acp-9-1621-2009, 2009. 22119

Gray, L. J., Beer, J., Geller, M., Haigh, J. D., Lockwood, M., Matthes, K., Cubasch, U., Fleitmann, D., Harrison, G., Hood, L., Luterbacher, J., Meehl, G. A., Shindell, D., van

ACPD
14, 22117–22153, 2014

Geel, B., and White, W.: Solar influences on climate, Rev. Geophys., 48, RG4001, doi:10.1029/2009RG000282, 2010. 22120, 22125
Grise, K. M. and Thompson, D. W.: Equatorial planetary waves and their signature in atmospheric variability, J. Atmos. Sci., 69, 857–874, doi:10.1175/JAS-D-11-0123.1, 2012. 22120
Grise, K. M. and Thompson, D. W.: On the signatures of equatorial and extratropical wave forcing in tropical tropopause layer temperatures, J. Atmos. Sci., 70, 1084–1102, doi:10.1175/JAS-D-12-0163.1, 2013. 22119, 22120
Hansen, F., Matthes, K., and Gray, L.: Sensitivity of stratospheric dynamics and chemistry to QBO nudging width in the chemistry–climate model WACCM, J. Geophys. Res., 118, 10–464, doi:10.1002/jgrd.50812, 2013. 22122
Kawatani, Y. and Hamilton, K.: Weakened stratospheric quasibiennial oscillation driven by increased tropical mean upwelling, Nature, 497, 478–481, doi:10.1038/nature12140, 2013. 22135
Kosaka, Y. and Xie, S.-P.: Recent global-warming hiatus tied to equatorial Pacific surface cooling, Nature, 501, 403–407, doi:10.1038/nature12534, 2013. 22136
Lean, J., Rottman, G., Harder, J., and Kopp, G.: SORCE contributions to new understanding of global change and solar variability, Sol. Phys., 230, 27–53, doi:10.1007/s11207-005-1527-2, 2005. 22122
Li, F., Austin, J., and Wilson, J.: The strength of the Brewer–Dobson circulation in a changing climate: coupled chemistry-climate model simulations, J. Climate, 21, 40–57, doi:10.1175/2007JCLI1663.1, 2008. 22119
Lin, P. and Fu, Q.: Changes in various branches of the Brewer–Dobson circulation from an ensemble of chemistry climate models, J. Geophys. Res., 118, 73–84, doi:10.1029/2012JD018813, 2013. 22120, 22133
Marsh, D. R., Mills, M. J., Kinnison, D. E., Lamarque, J.-F., Calvo, N., and Polvani, L. M.: Climate change from 1850 to 2005 simulated in CESM1 (WACCM), J. Climate, 26, 7372–7391, doi:10.1175/JCLI-D-12-00558.1, 2013. 22121, 22122, 22126, 22129
Matthes, K., Marsh, D. R., Garcia, R. R., Kinnison, D. E., Sassi, F., and Walters, S.: Role of the QBO in modulating the influence of the 11 year solar cycle on the atmosphere using constant forcings, J. Geophys. Res., 115, 18110, doi:10.1029/2009JD013020, 2010. 22122
Meehl, G. A., Washington, W. M., Arblaster, J. M., Hu, A., Teng, H., Tebaldi, C., Sanderson, B. N., Lamarque, J.-F., Conley, A., Strand, W. G., and White, J. B.: Climate system response

ACPD
14, 22117–22153, 2014

to external forcings and climate change projections in CCSM4, J. Climate, 25, 3661–3683, doi:10.1175/JCLI-D-11-00240.1, 2012. 22126

Meinshausen, M., Smith, S. J., Calvin, K., Daniel, J. S., Kainuma, M. L. T., Lamarque, J.-F., Matsumoto, K., Montzka, S., Raper, S., Riahi, K., Thomson, A., Velders, G. J. M., and van Vuuren, D. P.: The RCP greenhouse gas concentrations and their extensions from 1765 to 2300, Climatic Change, 109, 213–241, doi:10.1007/s10584-011-0156-z, 2011. 22122

Morgenstern, O., Giorgetta, M. A., Shibata, K., Eyring, V., Waugh, D. W., Shepherd, T. G., Akiyoshi, H., Austin, J., Baumgaertner, A. J. G., Bekki, S., Braesicke, P., Brühl, C., Chipperfield, M. P., Cugnet, D., Dameris, M., Dhomse, S., Frith, S. M., Garny, H., Gettelman, A., Hardiman, S. C., Hegglin, M. I., Jöckel, P., Kinnison, D. E., Lamarque, J.-F., Mancini, E., Manzini, E., Marchand, M., Michou, M., Nakamura, T., Nielsen, J. E., Olivié, D., Pitari, G., Plummer, D. A., Rozanov, E., Scinocca, J. F., Smale, D., Teyssèdre, H., Toohey, M., Tian, W., and Yamashita, Y.: Review of the formulation of present-generation stratospheric chemistry-climate models and associated external forcings, J. Geophys. Res., 115, D00M02, doi:10.1029/2009JD013728, 2010. 22122, 22129

Neely, R. R., Toon, O. B., Solomon, S., Vernier, J. P., Alvarez, C., English, J. M., Rosenlof, K. H., Mills, M. J., Bardeen, C. G., Daniel, J. S., and Thayer, J. P.: Recent anthropogenic increases in SO_2 from Asia have minimal impact on stratospheric aerosol, Geophys. Res. Lett., 40, 999–1004, doi:10.1002/grl.50263, 2013. 22127

Oberländer, S., Langematz, U., and Meul, S.: Unraveling impact factors for future changes in the Brewer–Dobson circulation, J. Geophys. Res., 118, 10–296, doi:10.1002/jgrd.50775, 2013. 22120, 22134

Randel, W. J. and Jensen, E. J.: Physical processes in the tropical tropopause layer and their roles in a changing climate, Nat. Geosci., 6, 169–176, doi:10.1038/ngeo1733, 2013. 22119

Randel, W. J., Shine, K. P., Austin, J., Barnett, J., Claud, C., Gillett, N. P., Keckhut, P., Langematz, U., Lin, R., Long, C., Mears, C., Miller, A., Nash, J., Seidel, D. J., Thompson, D. W. J., Wu, F., and Yoden, S.: An update of observed stratospheric temperature trends, J. Geophys. Res., 114, D02107, doi:10.1029/2008JD010421, 2009. 22135

Schmidt, T., Wickert, J., and Haser, A.: Variability of the upper troposphere and lower stratosphere observed with GPS radio occultation bending angles and temperatures, Adv. Space. Res., 46, 150–161, doi:10.1016/j.asr.2010.01.021, 2010. 22119, 22127

ACPD
14, 22117–22153, 2014

Shepherd, T. G. and McLandress, C.: A robust mechanism for strengthening of the Brewer–Dobson circulation in response to climate change: critical-layer control of subtropical wave breaking, J. Atmos. Sci., 68, 784–797, doi:10.1175/2010JAS3608.1, 2011. 22120

Simpson, I. R., Blackburn, M., and Haigh, J. D.: The role of eddies in driving the tropospheric response to stratospheric heating perturbations, J. Atmos. Sci., 66, 1347–1365, doi:10.1175/2008JAS2758.1, 2009. 22119

Solomon, S., Rosenlof, K. H., Portmann, R. W., Daniel, J. S., Davis, S. M., Sanford, T. J., and Plattner, G.-K.: Contributions of stratospheric water vapor to decadal changes in the rate of global warming, Science, 327, 1219–1223, doi:10.1126/science.1182488, 2010. 22119, 22120, 22127

SPARC-CCMVal: SPARC Report on the Evaluation of Chemistry-Climate Models, SPARC Report 5, WCRP-132, WMO/TD-1526, 2010. 22119, 22120, 22121, 22122

Stiller, G. P., von Clarmann, T., Haenel, F., Funke, B., Glatthor, N., Grabowski, U., Kellmann, S., Kiefer, M., Linden, A., Lossow, S., and López-Puertas, M.: Observed temporal evolution of global mean age of stratospheric air for the 2002 to 2010 period, Atmos. Chem. Phys., 12, 3311–3331, doi:10.5194/acp-12-3311-2012, 2012. 22119

Wang, W., Matthes, K., Schmidt, T., and Neef, L.: Recent variability of the tropical tropopause inversion layer, Geophys. Res. Lett., 40, 6308–6313, doi:10.1002/2013GL058350, 2013. 22119, 22121, 22123, 22127, 22130

Wigley, T.: Appendix A: Statistical issues regarding trends, in: Temperature Trends in the Lower Atmosphere: Steps for Understanding and Reconciling Differences, edited by: Karl, T. R., Hassol, S. J., Miller, C. D., and Murray, W. L., A Report by Climate Change Science Program and the Subcommittee on Global Change Research, Washington, DC, USA, UNT Digital Library, 129–139, 2006. 22124

Zhou, X.-L., Geller, M. A., and Zhang, M.: Cooling trend of the tropical cold point tropopause temperatures and its implications, J. Geophys. Res., 106, 1511–1522, doi:10.1029/2000JD900472, 2001. 22121

ACPD
14, 22117–22153, 2014

Table 1. Overview of fully-coupled CESM-WACCM simulations (1955–2099).

Simulations	Natural Forcings	GHGs
Natural	All natural forcings, including transit solar variability, fully coupled ocean, prescribed volcanic aerosols and nudged QBO	Fixed GHGs to 1960s state
SolarMean	As Natural run, but with fixed solar radiation	Fixed
FixedSST	As Natural run, but with fixed SSTs	Fixed
NOQBO	As Natural run, but without QBO nudging	Fixed
RCP85	As Natural run	RCP8.5 scenario

ACPD
14, 22117–22153, 2014

Table 2. Overview of WACCM atmospheric stand-alone simulations (2001–2010).

Simulations	Ensemble Numbers	Vertical levels	Forcings	Stratospheric aerosols
W_L103	3	103	Observed solar variability and SSTs, nudged QBO, GHGs in RCP4.5 scenario	Volcanic aerosols from CCMVal-2
W_L66	3	66	As W_L103	As W_L103
W_Aerosol	1	103	As W_L103	Stratospheric aerosols from CCMI

ACPD
14, 22117–22153, 2014

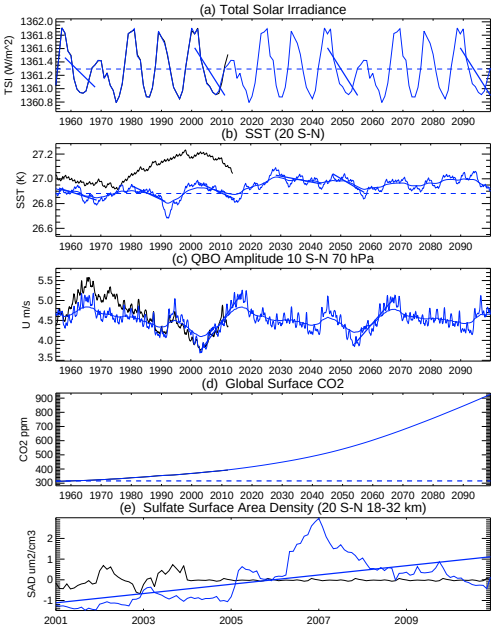

Figure 1. Time series of forcing data sets used for the simulations from 1955 through 2100. **(a)** TSI from observations (black) until 2012, the *Natural* run (solid blue) and the *SolarMean* run (dashed blue). The last four solar cycles have been repeated into the future. **(b)** SSTs from observations HadISSTs (see details in text) (black), the *Natural* run (solid blue) and the *FixedSST* run (dashed blue). The SSTs in observations and the *Natural* run have been smoothed by a low-pass ($T > 30$ years) Butterworth Filter. The smooth blue line has been smoothed twice by the same low-pass Butterworth Filter. **(c)** Same as in **(b)**, but for the QBO amplitude calculated from zonal mean zonal winds at 70 hPa and between 10° S and 10° N. **(d)** Global surface CO_2 concentration from observations (black, overlapped with the blue line), the *RCP85* run (solid blue) and the *Natural* run (dashed blue). **(e)** AOD (532 nm, 18–32 km) from the CCMI (Solid blue) and the CCMVal2 (black) projects for the time 2001–2010. The blue solid straight lines in each subfigure are the linear fits of the respective forcing for the selected decade.

ACPD
14, 22117–22153, 2014

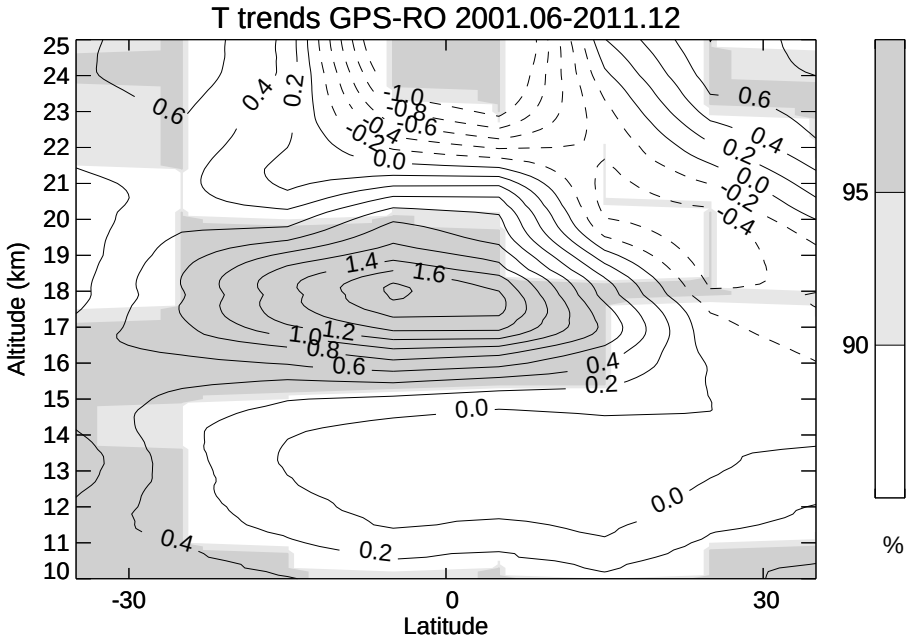

Figure 2. Latitude-height section of linear temperature trends over the past decade (2001–2011) from *GPS-RO* data over a height range from 10 to 25 km and 35° S to 35° N latitude; contour interval: 0.3 K decade^{-1}. Grey shading represents the statistical significance for the trends. See text for details on the linear trend and the statistical significance calculation.

ACPD
14, 22117–22153, 2014

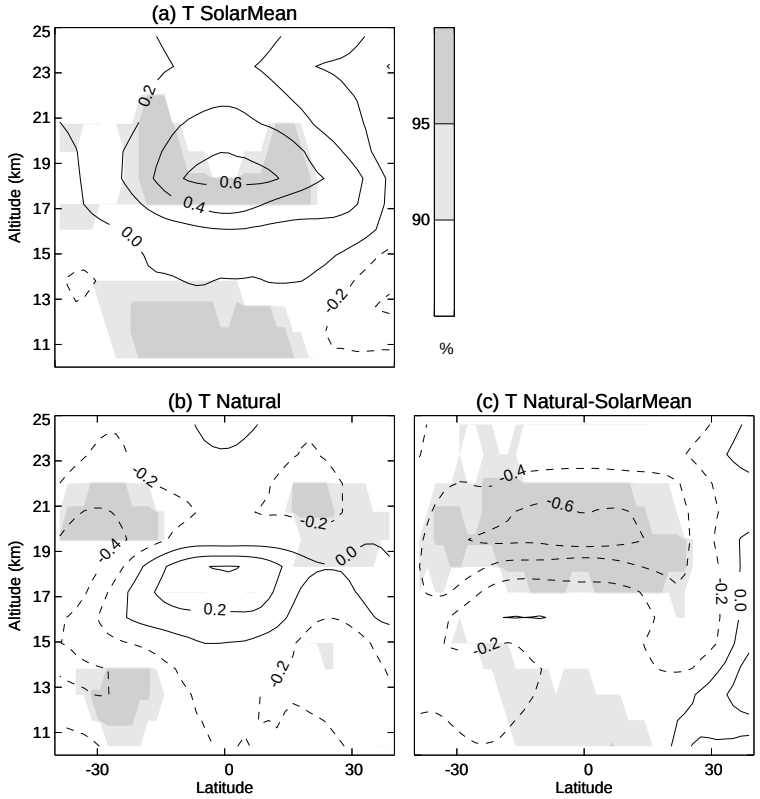

Figure 3. (a, b) Latitude-height sections of composite temperature trends over selected time periods (1958–1968, 2001–2011, 2045–2055, and 2089–2099, see Fig. 1) from the *Natural* and *SolarMean* runs, respectively; contour interval: 0.2 K decade^{-1}. **(c)** The differences between **(a)** and **(b)**. Grey shading represents statistically significant trends (differences). See text for details on the calculation of the composite trend and the trend differences, and the testing of the statistical significance for both of the composite trend and the trend differences.

ACPD
14, 22117–22153, 2014

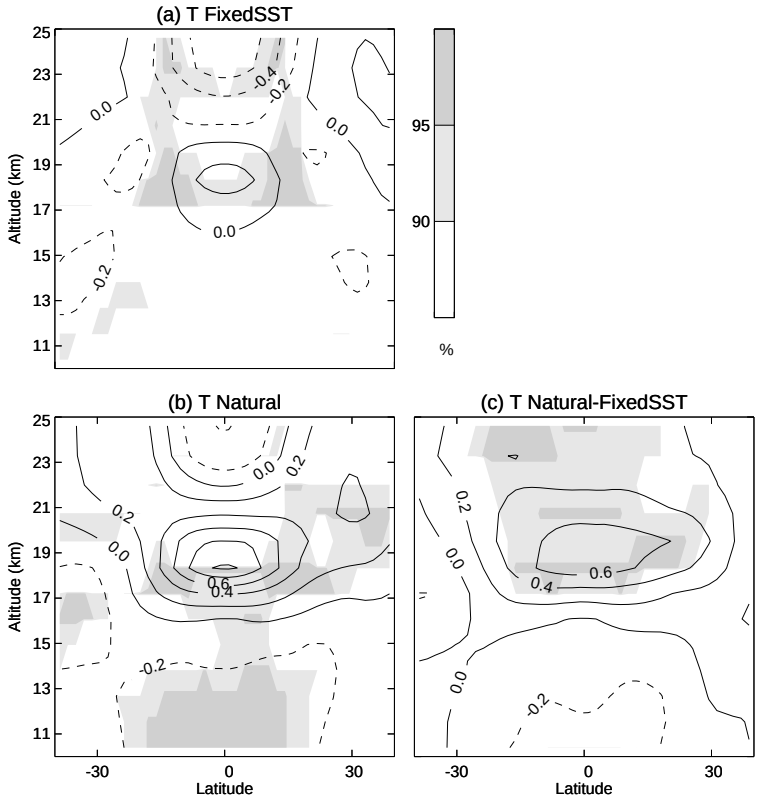

Figure 4. (a, b) Latitude-height sections of composite temperature trends over selected time periods (1956–1968, 1980–1991, 2001–2014, 2028–2043, 2047–2057, see Fig. 1) from the *Natural* and *FixedSST* runs, respectively; contour interval: 0.2 K decade^{-1}. **(c)** The differences between **(a)** and **(b)**. Grey shading as in Fig. 3.

ACPD
14, 22117–22153, 2014

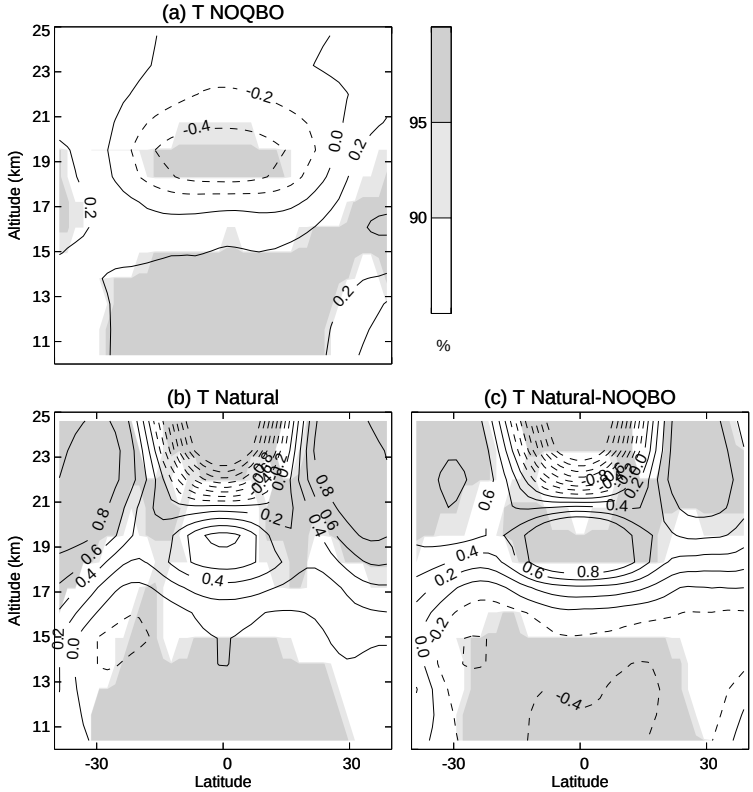

Figure 5. Same as Fig. 3, but for the impact of the QBO amplitude on temperature trends **(c)** by comparing the *Natural* and the *NOQBO* experiments **(a, b)** for the periods 2003–2017 and 2054–2068 (see Fig. 1); contour interval: 0.2 K decade^{-1}.

ACPD
14, 22117–22153, 2014

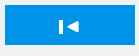

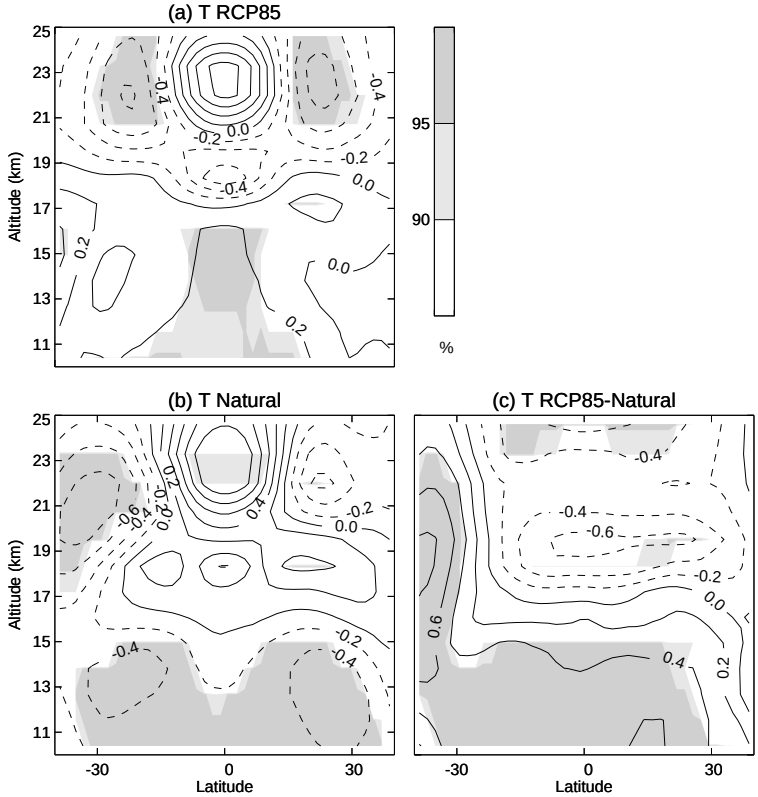

Figure 6. Same as Fig. 3, but for the impact of anthropogenic forcings (GHGs and ODS) on temperature trends by comparing the *Natural* and *RCP85* experiments **(a, b)** for the period 2001–2011; contour interval: 0.2 K decade^{-1}.

ACPD
14, 22117–22153, 2014

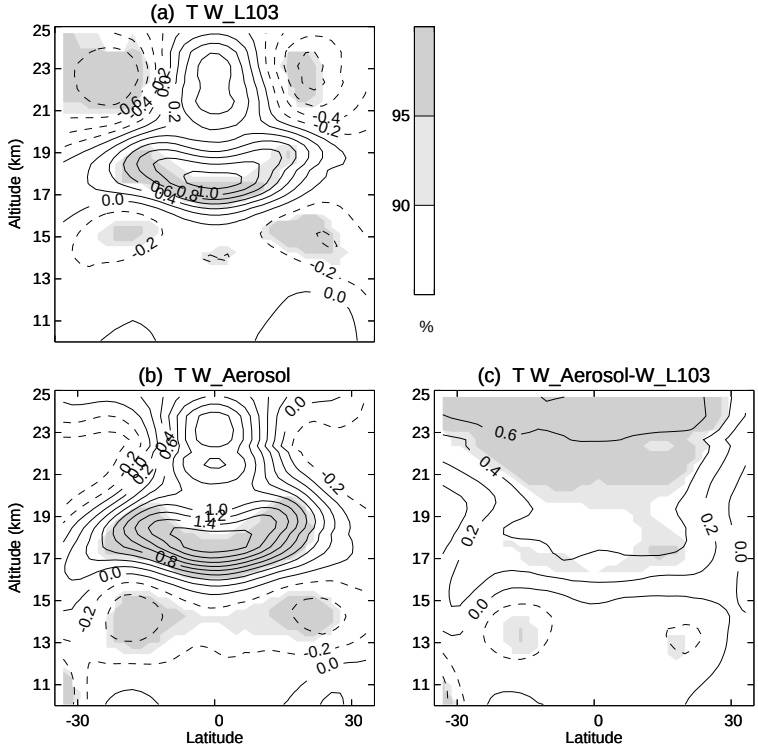

Figure 7. Same as Fig. 3, but for the impact of stratospheric aerosols on temperature trends by comparing the *W_L103* and the *W_Aerosol* experiment **(a, b)** for the period 2001–2010; contour interval: 0.2 K decade^{-1}.

ACPD
14, 22117–22153, 2014

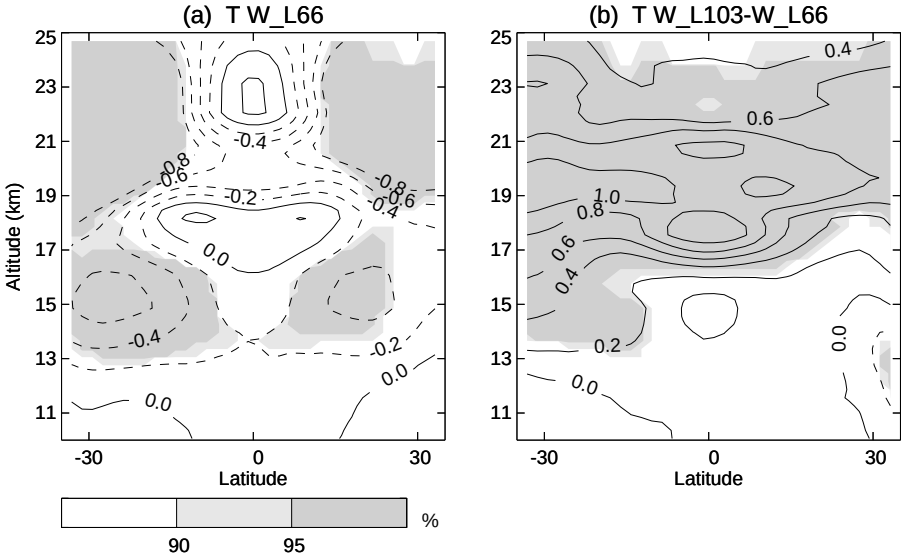

Figure 8. (a) Latitude-height sections of temperature trends between 2001 and 2010 from the ensemble of the *W_L66* experiment to investigate the impact of the differences in vertical resolution; contour interval: 0.2 K decade^{-1} and grey shading as in Fig. 3. **(b)** The differences between (Figs. 7a and 8a).

ACPD
14, 22117–22153, 2014

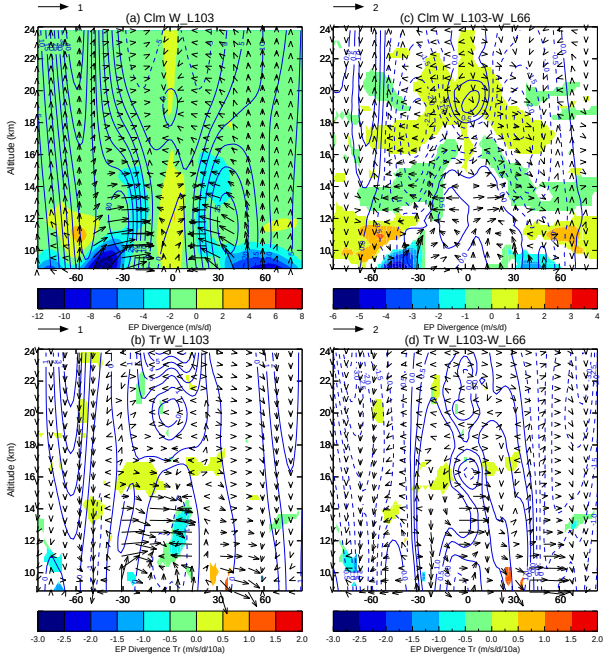

Figure 9. (a) Annual mean climatological zonal mean zonal wind (contours, contour interval 5 m s^{-1}, dashed lines indicate easterly winds, the thick line is the zero wind line), EP flux vector (arrows, scaled with the square root of pressure) and its divergence (shading, positive values indicate divergence) for the *W_L103* experiment from 8 to 25 km and 80° S through 80° N. **(c)** Differences of the zonal mean zonal wind (contour interval 0.5 m s^{-1}), EP flux vector and its divergence (colour shadings indicate 95 % statistical significances) between the *W_L103* and the *W_L66* experiments. (**b** and **d**) Same as **(a)** and **(c)**, but for the linear trends from 2001 to 2010. The shadings in **(b)** indicate 95 % statistical significance. The shadings in **(d)** indicate 95 % statistical significance in both **(b)** and **(c)**. The contour intervals are 1 m s^{-1} and 0.5 m s^{-1} in **(c)** and **(d)**, respectively.

ACPD
14, 22117–22153, 2014

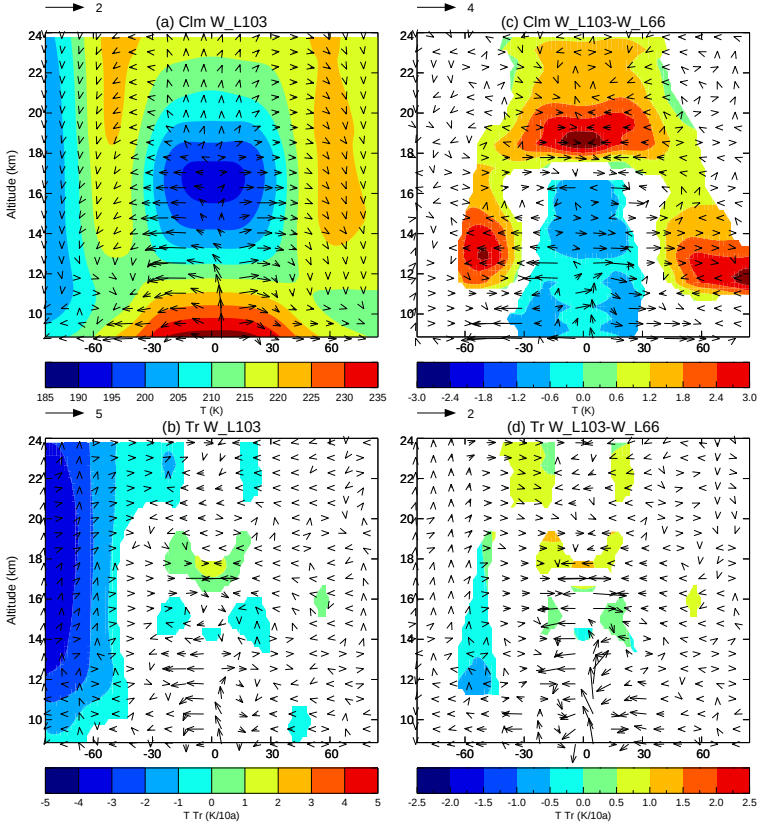

Figure 10. Same as Fig. 9, but for the vertical and meridional components of the residual circulation (arrows) and the zonal mean temperature (shading).

ACPD
14, 22117–22153, 2014